Ion beam synthesis of planar opto-electronic devices

A. Polman *, E. Snoeks, G.N. van den Hoven, M.L. Brongersma, R. Serna,
J.H. Shin, P. Kik, E. Radius

FOM-Institute for Atomic and Molecular Physics, Kruislaan 407, 1098 SJ Amsterdam, The Netherlands

Abstract

Photonic technology requires the modification and synthesis of new materials and devices for the generation, guiding, switching, multiplexing and amplification of light. This paper reviews how some of these devices may be made using ion beam synthesis. Special attention is paid to the fabrication of erbium-doped optical waveguides.

1. Introduction

Photonics is an emerging technology in the present information era [1]. Using optical data transfer, extremely high data transmission rates can be achieved, much higher than by using electronic transmission. This new technology requires the modification and synthesis of new materials for guiding, switching, multiplexing and amplification of light, as well as for light sources such as lasers and LEDs. While at present most optical communication takes place through optical fibers for long distance data transfer, in the future local signal transfer and processing may also take place in the optical domain. This can be achieved using integrated planar opto-electronic devices [2]. When such devices are integrated on a Si substrate, opto-electronic integration may become a reality.

Fig. 1 shows a schematic of a planar waveguide on a Si substrate, which may be used for on-chip optical communication [3]. First, a SiO_2 buffer layer is thermally grown on the Si wafer, after which a layer with slightly higher refractive index (e.g. phosphosilicate glass) is deposited. Subsequently, ridges are created using standard photolithography and etching techniques, and finally an SiO_2 cladding layer is deposited. Typical wavelengths at which these waveguides should be designed are 1.5 μm (coinciding with the transmission maximum of standard silica fiber), 1.3 μm (coinciding with the dispersion minimum of silica fiber), or 0.8–0.9 μm (at which inexpensive commercial semiconductor lasers are available). In the future, operation in the visible will also become important, e.g. in applica-

tions integrated with polymer fibers, which are not transparent in the infrared.

Fig. 2 shows a schematic of a planar photonic integrated circuit which includes a variety of opto-electronic devices, connected by optical waveguides. The device itself does not have any functionality, but is meant to illustrate how several opto-electronic functions could be integrated on a single Si chip. The various devices, which can in principle all be fabricated using ion implantation, will be discussed hereafter. Note that most of these devices have not been demonstrated yet; Fig. 2 is literally science fiction.

1.1. Erbium-doped Si light emitting diode

An important element in a photonic integrated circuit is the light source. For opto-electronic integration it would be interesting to have a light source based on Si. Unfortunately, due to its indirect bandgap, Si shows very inefficient band-to-band transitions. Recent work has shown that light emission from silicon can be achieved by implantation with erbium ions [4–9]. Trivalent Er shows an optical transition at 1.54 μm. In Si, electron–hole pairs can recombine near an Er ion and transfer their recombination energy to the Er ion. The Er can then decay by the emission of a 1.54 μm photon. A large research effort has been devoted in the past few years to the incorporation of Er in a variety of Si-based materials using ion implantation. Photoluminescence [5,6] and electroluminescence [7–9] at 1.54 μm have been observed at room temperature, and impact excitation of Er has also been shown [7,9]. The key to this success was the engineering of the local environment of the Er ion by the addition of impurities such as oxygen [5]. Recent work focusses on optimizing the luminescence efficiency and developing a further

---

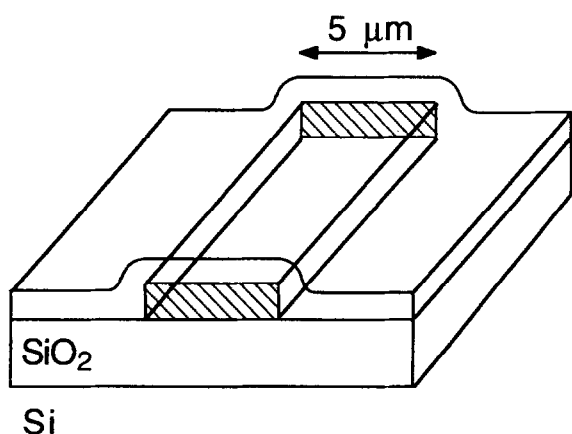* Corresponding author. Fax +31-20-6684106, tel. +31-20-6081234, e-mail: polman@amolf.nl.

Fig. 1. Schematic cross section of a planar optical waveguide on Si. The cross-hatched region is the high-index core of the waveguide.
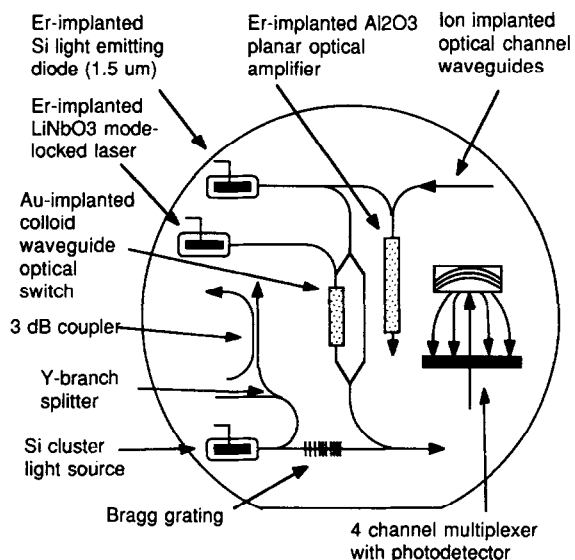

Fig. 2. Science fiction. Schematic of photonic integrated circuit with various integrated optical devices.

understanding of the excitation process of Er in Si. In the future, other rare earths may also be implanted into Si to obtain emission at other wavelengths.

1.2. Si cluster light source

An alternative way to achieve light emission from Si is by engineering the electronic band structure. For example, nanometer-size Si clusters may show enhanced optical emission, compared to bulk Si, due to a quantum size effect. Similar effects have been observed in electrochemically etched porous Si. The advantage of Si nanoclusters is that they can be embedded in an insulating SiO_2 layer and hence integrated in standard

Si devices. Si clusters can be made by Si implantation into SiO_2, creating a supersaturated Si solution. Upon thermal annealing, small Si nanoclusters precipitate, of which the size depends on the precise annealing temperature and time [10,11]. Fig. 3 shows an example of a room-temperature photoluminescence (PL) spectrum of a thermally grown SiO_2 film on Si, implanted at room temperature with 5×10^{16} Si/cm^2 at 175 keV. PL spectroscopy measurements were performed using an Ar ion laser (488 nm) as a pump source. Clear luminescence around 700–800 nm is observed after annealing for 10 min at 700°C. The luminescence intensity increases when an additional anneal at 100°C is performed for 12 h. A slight redshift is also observed, which would be consistent with an increase in cluster size upon annealing. Present work focusses on the search for a correlation between cluster size and optical properties, as well as the attainment of efficient electroluminescence by carrier injection in the Si clusters. If high enough quantum efficiencies can be achieved, it may be possible to fabricate a LED or even a laser based on Si clusters.

1.3. Planar optical waveguides and passive devices

Once the light is generated, it should be guided over the substrate using optical waveguides. SiO_2 is a transparent waveguide material that can easily be deposited onto Si. Various methods to fabricate optical waveguides in SiO_2 using ion implantation have been demonstrated. Ion irradiation causes densification of the silica network, thereby increasing the refractive index and creating an optical waveguide [12]. Impurities that increase the index, such as e.g. N, may also be implanted in SiO_2. Focussed ion beams are also being
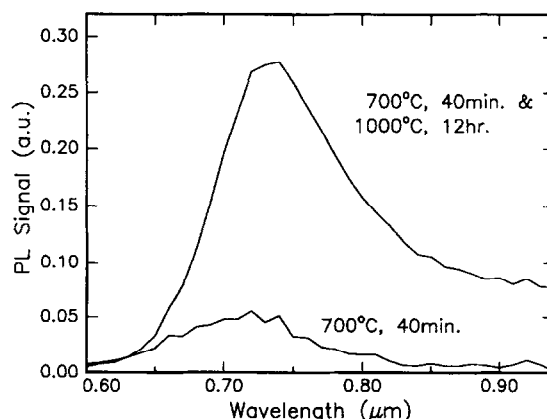

Fig. 3. Room-temperature photoluminescence spectra of Si-implanted SiO_2 (175 KeV, 5×10^{16} Si/cm^2). Spectra were taken after annealing in vacuum at 700°C (40 min) and after a subsequent anneal at 1000°C (12 h), $\lambda_{pump} = 488$ nm. (From Brongersma et al., Ref. [11].)

used to fabricate localized index contrasts in SiO_2 [13]. As an alternative to ion implantation, optical waveguide films may be deposited on a Si substrate [3] (as in Fig. 1); the light may then be coupled into devices in the wafer using integrated mirrors. Once the waveguide technology is established, a variety of passive devices can be made, such as splitters, couplers, gratings and multiplexers (see Fig. 2). As Si is transparent at the telecommunication wavelengths 1.3 and 1.5 μm, waveguides may also be fabricated in the Si substrate. Index contrasts may be made in Si by e.g. Ge implantation.

1.4. Planar optical amplifier

Once the light is generated and guided over the wafer, optical losses take place, either intrinsic to the waveguides, or in devices such as splitters and multiplexers. To compensate for these losses, the light intensity has to be amplified. This can be done in a planar optical amplifier which contains an optical dopant with the proper optical transition. For example, light at 1.5 μm may be amplified in an Er-doped planar waveguide. A continuous-wave pump laser is required to excite the Er. An optical signal at 1.5 μm may then be amplified by stimulated emission, if a high enough inversion of the Er can be reached. Some of the material issues in the fabrication of such waveguide amplifiers will be shown later on in this paper.

1.5. Optical switch

For fast optical signal processing the light needs to be switched at high frequency. This can be done in a so-called Mach–Zehnder geometry [2], in which the refractive index in one of the branches of an interferometer structure is modulated, leading to either constructive or destructive interference, i.e. optical switching (see Fig. 2). Such index modulations can be made in $LiNbO_3$, a material with a relatively strong electro-optic effect. Recent experiments focus on the deposition of $LiNbO_3$ films using e.g. laser-ablation [14]. Erbium ion implantation of $LiNbO_3$ has been performed to fabricate an optical amplifier in $LiNbO_3$, to compensate for losses in the Mach–Zehnder structure. Several interesting material issues in relation to the amorphization, recrystallization and diffusion of Er in Er-implanted $LiNbO_3$ have already been studied [15,16].

An alternative way to modulate the index is by a non-linear effect in e.g. a waveguide doped with metal colloids. Nanometer-size metallic clusters can show non-linear optical properties due to plasma resonances in and at the surface of the clusters. Therefore, if a laser is used to excite these clusters, the index in the waveguide may be changed and an optical signal switched. The typical wavelength range in which these non-linear effects are efficient is 350–500 nm. The

synthesis of nanometer-size metallic clusters using ion implantation has been demonstrated in a variety of materials [17–19], but optical switching using these clusters has not been demonstrated.

1.6. Detector

After generation, propagation and optical processing, the optical signal has to be detected. For signal wavelengths below 1.1 μm (i.e. energies above the Si bandgap) detectors based on Si are readily available. This wavelength range can be extended into the infrared by co-doping with Ge (bandgap 0.67 eV, 1.85 μm) [20], and extended further into the infrared using e.g. SnGe composites [21]. The advantage of Si-based detectors is that they can be integrated with other electrical functions on the same chip, so that opto-electronic integration becomes possible.

The previous section is meant to illustrate various possible opto-electronic devices which may be fabricated using ion implantation. As only a few of them have been realized so far, we end this section with the conclusion that an enormous challenge remains to investigate the material issues related to all of these devices.

2. Er-doped optical gain materials

2.1. Soda-lime silicate glass

In this section we will show recent experimental results on the ion beam synthesis of Er-doped optical waveguide materials operating at 1.5 μm. Er-doped waveguide amplifiers can be used for example to compensate for losses in a Y-branch (1-to-2) splitter. In this case an optical gain of a factor 2 (3 dB) is required. To obtain such a gain in a waveguide of typically a few cm length, Er concentrations of the order of 0.5 at.% are required. First, we have doped soda-lime silicate glass with Er using ion implantation. The advantage of this glass is that single-mode optical waveguides can be made using the relatively simple Na^+–K^+ ion exchange process from a KNO_3 melt. In this way, Na ions near the surface are replaced by K, thereby raising the refractive index in a typically 6 μm thick surface layer. Such waveguides are compatible with standard single-mode silica fibers as far as both the mode diameter and the refractive index are concerned.

Fig. 4 shows a PL spectrum of the Er-implanted silica glass (500 keV, 3.7×10^{15} Er/cm^2) after annealing at 512°C [22]. Annealing is necessary to remove implantation-induced defects which, by an interaction with the Er^{3+} ions, reduce the luminescence lifetime and efficiency [23]. PL measurements are done using an Ar ion laser at 514.5 nm as a pump source. This
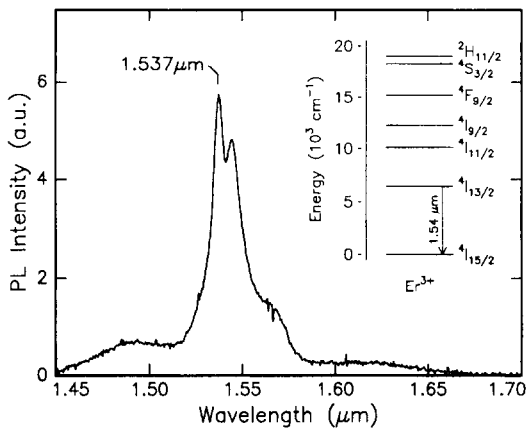
Fig. 4. Photoluminescence spectrum of Er-implanted soda-lime silicate glass (500 keV, 3.7×10^{15} Er/cm^2) after thermal annealing at 512°C for 1 h. The inset shows the energy level diagram of Er^{3+}. (From Snoeks et al., Ref [2].)

wavelength is resonantly absorbed at the $^2H_{11/2}$ manifold of the Er^{3+} ion (see inset in Fig. 4). After rapid non-radiative relaxation to the $^4I_{13/2}$ level, the Er decays to the ground state by emission of a 1.54 μm photon. The spectrum in Fig. 4 is relatively broad due to Stark splitting of the degenerate 4f levels in the electric field around the Er ion, as well as due to inhomogeneous broadening as a result of the broad distribution of sites of Er in the multicomponent glass.

Fig. 5 shows PL lifetime measurements at 1.54 μm of Er in soda-lime glass as a function of Er peak concentration, measured after annealing at 512°C [24]. The maximum concentration in Fig. 5 corresponds to a fluence of 1.8×10^{16} Er/cm^2. As can be seen, a linear
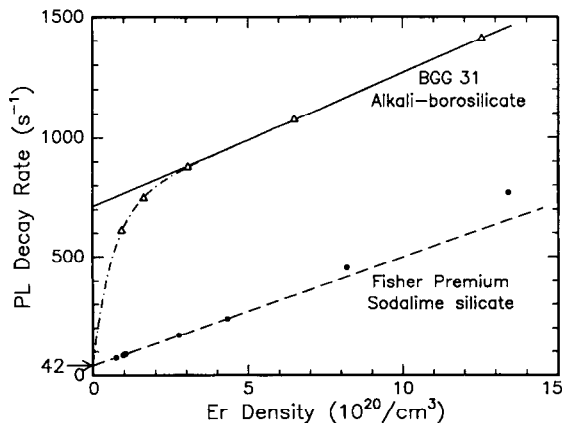

Fig. 5. Photoluminescence decay rate at 1.54 μm as a function of Er peak concentration for Er-implanted soda-lime silicate glass (500 keV, annealed at 512°C) and borosilicate glass (400 keV, annealed at 400°C). The lines are fits to concentration quenching models discussed in the text. (From Snoeks et al., Ref. [22].)

increase of the decay rate is observed. This effect is attributed to a concentration quenching effect: at high Er concentrations energy transfer can take place between an excited and an unexcited Er ion. This migration continues until a quenching center is met and the excitation is lost. This effect becomes stronger at higher Er concentration and results in an increase in the PL decay rate. In soda-lime glass, infrared absorption measurements have shown the presence of 8×10^{18} OH/cm^3 [24]. OH groups are important quenching centers as the energy of the second harmonic of the OH stretch vibration corresponds to the 1.5 μm transition energy of Er^{3+}. In a simple concentration quenching model the PL decay rate W_0 as a function of Er concentration N_{Er} is given by

$$W_0 = W_{rad} + W_i + C_{Er-Er} N_q N_{Er} \qquad (1)$$

with W_{rad} the radiative decay rate of Er, W_i the internal non-radiative decay rate of each Er ion, C_{Er-Er} an interaction constant, and N_q the density of quenching sites. The linear behavior as a function of N_{Er} predicted by Eq. (1) describes the data for soda-lime glass in Fig. 5 quite well. The intercept at zero Er concentration found in Fig. 5 is 42 s^{-1} (24 ms), close to the radiative decay rate W_{rad} found in an independent experiment [25]. This implies that in Er-implanted soda-lime glass $W_i = 0$, i.e. after thermal annealing no implantation-induced structural defects remain that couple directly to the Er.

Fig. 5 also shows data for 400 keV Er implanted alkali-borosilicate glass. This glass was annealed at 400°C, the temperature at which the maximum PL intensity was obtained. For all Er concentrations the Er decay rate is much higher than for the soda-lime glass. For concentrations above 3×10^{20} Er/cm^3 the behavior can be described by Eq. (1). Indeed, borosilicate glass contains OH quenching impurities, as determined by infrared absorption spectroscopy [24]. For low concentrations (or planted fluences) a non-linear behavior is found. This can be explained assuming that in this glass radiation damage caused by the ion beam induces additional quenching of the Er by an increase of the internal quench rate W_i. The dash-dotted line through the data is based on a calculation [24] in which it is assumed that the damage coupling to the Er increases with Er fluence according to an overlap model, i.e. W_i is proportional to $1 - \exp(\phi/\phi_c)$ with ϕ_c a critical fluence. It is interesting to note that radiation damage is still present in this borosilicate glass even after annealing at 400°C. This is consistent with earlier observations that the presence of B in the silica network results in rather stable radiation damage, due to electronic energy loss processes [26].

The concentration quenching behavior shown in Fig. 5 is a limitation for the application of these silicate

glasses. For the typical Er concentrations required in an amplifier (3×10^{20} Er/cm^3) the PL lifetime is around 5 ms in soda-lime glass and 1 ms in the borosilicate. These lifetimes are much lower than the purely radiative lifetimes at 24 ms. As a result, much higher pump powers are required to reach inversion in such Er-doped waveguides. A further disadvantage of these Na–K ion-exchanged waveguides is that the optical mode profiles are relatively wide (6–10 μm). Therefore, relatively high pump powers are required to reach high pump intensities in the Er-doped part of the waveguides.

2.2. Al_2O_3

Waveguides with better confined modes can be made in Al_2O_3 [27]. A 600 nm thick polycrystalline Al_2O_3 film was first deposited on an oxidized Si substrate by radio-frequency sputter deposition. It was then implanted with 1.6×10^{16} Er/cm^2 1.3 MeV Er (peak concentration 1.4 at.%). Subsequently, a ridge was etched using reactive ion etching, a silica cladding was deposited, and the structure was annealed at 825°C. Annealing is necessary to reduce the waveguide losses and optimize the Er active fraction as well as the luminescence lifetime [28]. Er luminescence lifetimes at 1.54 μm as long as 10 ms can be obtained in these polycrystalline Al_2O_3 films at Er concentrations as high as 1 at.%. This implies that the concentration quenching phenomena observed in the silica glasses are not present in Al_2O_3.

Fig. 6 shows an optical gain measurement on a 9 mm long Er-implanted Al_2O_3 waveguide [29]. The waveguide was pumped using an AlGaAsP laser operating at 1.48 μm. At the same time, a signal at 1.53 μm was propagated through the waveguide, and the signal transmissio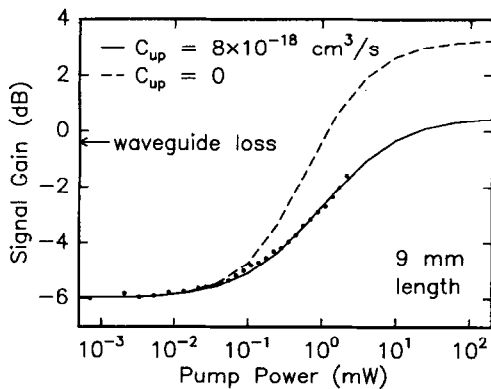n change as a function of pump power was measured. Without pump, a signal absorption of 6 dB is found, due to the Er (5.6 dB) as well as a small waveguide loss (0.4 dB). As the pump power is increased, and thereby the steady state excited Er population, less absorption takes place. However, for the maximum pump power used (3 mW in the waveguide) no net gain is observed. Also shown in Fig. 6 is a model calculation (dashed line), made using the known absorption and emission cross sections, Er lifetime, Er depth profile and optical mode profiles. As can be seen, the calculated gain is a much steeper function of pump power than the actually measured gain.

The origin of this difference becomes clear from Fig. 7 which shows a PL spectrum of the waveguide taken using a fiber which was positioned perpendicular to the surface of the waveguide, collecting the spontaneous fluorescence from the Er in the waveguide. The spectrum shows clear peaks at 522, 545, 660, 850 and 980 nm, apart from the Er luminescence at 1.54 μm. Note that the pump wavelength was 1.48 μm. The lower wavelength peaks are attributed to an upconversion process: at high pump powers higher lying levels of the Er ions (see inset in Fig. 4) are populated due to energy exchange between excited Er ions. Therefore, less Er is available for optical gain, as a significant fraction is continuously populated at these higher levels. Also, as a result of upconversion, the effective lifetime of the first excited state is reduced as the pump power is increased. The additional depopulation of the first excited state of Er^{3+} due to the upconversion effect can be described using an upconversion coefficient C_{up}:

$$W = W_0 + C_{up} \frac{(N_{Er}^*)^2}{N_{Er}},$$ (2)

with N^*_{Er} the concentration of Er in the $^4I_{13/2}$ level. Incorporating Eq. (2) and the effects of populating higher lying levels in the gain calculation [29], and fitting it to the data, yields the drawn line in Fig. 6. As can be seen, the maximum attainable gain at high pump power is 0.3 dB. The upconversion coefficient
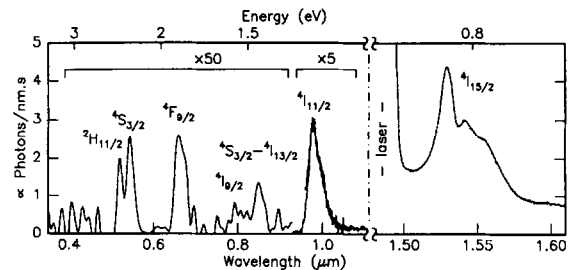

Fig. 6. Optical gain measurements (closed circles) in an Er-implanted (1.3 MeV, 1.6×10^{16} Er/cm^2) Al_2O_3 channel waveguide. $\lambda_{pump} = 1.48$ μm, $\lambda_{signal} = 1.532$ μm. The drawn line is a model calculation taking into account upconversion. The dashed line is a calculation for the case without upconversion. (From van den Hoven et al., Ref. [30].)

Fig. 7. Photoluminescence spectrum of the waveguide in Fig. 6. $\lambda_{pump} = 1.48$ μm, pump power in the waveguide = 2 mW. (From van den Hoven et al., Ref. [31].)

required to fit the data is $C_{up} = 8 \times 10^{-18}$ cm^3/s [29]. Measurements on upconversion in Er-implanted soda-lime silicate waveguides yielded $C_{up} = 3 \times 10^{-18}$ cm^3/s [30]. Both upconversion coefficients are so large that in an actual waveguide doped with Er to a concentration of typically 3×10^{20} Er/cm^3, the Er luminescence lifetime is fully dominated by decay due to upconversion, rather than spontaneous emission

Upconversion is an effect intrinsic to Er doping, of which the rate depends on the Er–Er distance, the spectral overlap between Er emission and absorption spectra, and the phonon spectrum of the host. Upconversion can only be avoided if the Er concentration is reduced. In fact, calculations for an Er-doped Al_2O_3 waveguide with a three times lower peak concentration as the one in Fig. 6, and using all known parameters including the value of C_{up} determined from Fig. 6, predict a maximum attainable net gain in Al_2O_3 planar waveguides pumped at 1.48 μm of 1 dB/cm. This implies that a 3 cm long waveguide is required to fabricate a loss-free Y-branch splitter. Note that, due to the high index contrast, Al_2O_3 waveguides can be rolled up in spirals (10 cm/mm^2) so that the final device will only take up a very small area.

Finally, we note that the upconversion effect can also be used in an advantageous way. We have doped a Y_2O_3 planar waveguide with Er by implantation. At an Er concentration of 0.75 at.%, much stronger upconversion is observed than in Al_2O_3 [31]. The reason is that the typical phonon energies in the heavy metal Y_2O_3 are lower than those in Al_2O_3. Therefore, nonradiative decay rates are relatively low, and the lifetimes of the excited states are quite long. As a result, upconversion is an efficient process. In fact, a third-order upconversion process leading to emission at 410 nm has been observed in Y_2O_3. The upconversion effect may be used to fabricate a planar upconversion laser operating in the visible.

3. Conclusions

Photonic integrated circuits involve a variety of opto-electronic devices for the generation, guiding, switching, multiplexing and amplification of light. Many of these devices can be made using ion implantation, but only few have been demonstrated. It is a challenge to the ion beam community to investigate the material issues related to these devices and to actually demonstrate the feasibility of their operation.

Acknowledgements

References

[1] See, e.g. Business Week (McGraw Hill, May 1993) p. 52.

[2] See e.g. J.T. Boyd, Ed., Integrated Optics: Devices and Applications (IEEE, New York, NY, 1990).

[3] See e.g. C.H. Henry, G.E. Blonder and R.F. Kazarinov, J. Lightwave Technol. 7 (1989) 1530.

[4] See e.g. A. Polman, G.N. van den Hoven, J.S. Custer, J.H. Shin and R. Serna, J. Appl. Phys. 77 (1995) 1256, and references therein.

[5] S. Coffa, G. Franzò, F. Priolo, A. Polman and R. Serna, Phys. Rev. B. 49 (1994) 16313.

[6] S. Lombardo, S.U. Compisano, G.N. van den Hoven, A. Cacciato and A. Polman, Appl Phys. Lett. 63 (1993) 1942.

[7] G. Franzò, F. Priolo, S. Coffa, A. Polman and A. Carnera, Appl. Phys. Lett. 64 (1994) 2235.

[8] F.Y.G. Ren, J. Michel, Q. Sun-Paduano, B. Zheng, H. Kitagawa, D.C. Jacobson, J.M. Poate and L.C. Kimerling, Mater. Res. Soc. Proc. 301 (1993) 87.

[9] S. Lombardo, S.U. Campisano, G.N. van den Hoven and A. Polman, J. Appl. Phys., 77 (1995) 6504.

[10] H.A. Atwater, K.V. Shcheglov, S.S. Wong, K.J. Vahala, R.C. Flagan, M.L. Brongersma and A. Polman, Mater. Res. Soc. Proc. 316 (1994) 409.

[11] M.L. Brongersma and A. Polman, to be published.

[12] See e.g. P.D. Townsend, Nucl. Instr. and Meth. B 46 (1990) 18.

[13] A. Roberts, M.L. von Bibra and J.N. Walford, these Proceedings (IBMM-95), Nucl. Instr. and Meth. B 106 (1995).

[14] S. Bauer, L. Beckers, M. Fleuster, J. Schubert, W. Zander, Ch. Buchal and B. Kabius, Mater. Res. Soc. Meeting, Proc. 392 (1995).

[15] M. Fleuster, Ch. Buchal, E. Snoeks and A. Polman. J. Appl. Phys. 75 (1994) 173.

[16] M. Fleuster, Ch. Buchal, E. Snoeks and A. Polman, Appl. Phys. Lett. 65 (1994) 225.

[17] K. Fukumi, A. Chayahara, K. Kadono, T. Sakaguchi, Y. Horino, M. Miya, J. Hayakawa and M. Satou, Jpn. J. Appl. Phys. 30 (1991) L742.

[18] R.F. Haglund, R.H. Magruder, S.H. Morgan, D.O. Henderson, R.A. Weller, L. Yang and R.A. Zuhr, Nucl. Instr. and Meth. B 65 (1992) 405.

[19] C.W. White, D.S. Zhou, J.D. Budai, R.A. Zuhr, R.H. Magruder and D.H. Osborne, Mater. Res. Soc. Proc. 316 (1994).

[20] See e.g. S. Luryi, T.P. Pearsal, H. Temkin and J.C. Bean, IEEE Electron.Device Lett. EDL-7 (1986) 104.

[21] G. He, M.E. Taylor, K. Saipetch and H.A. Atwater, presented at 9th Int. Conf. on Ion Beam Modification of Materials, Canberra, Australia (1995), to be published.

[22] E. Snoeks, G.N. van den Hoven and A. Polman, J. Appl. Phys. 75 (1994) 2644.

[23] A. Polman and J.M. Poate, J. Appl. Phys. 73 (1993) 1669.

[24] E. Snoeks, P. Kik and A. Polman, Opt. Mater., submitted.

[25] E. Snoeks, A. Lagendjik and A. Polman, Phys. Rev. Lett. 74 (1995) 2459.

[26] D.L. Griscom, G.N. Sigel Jr. and R.J. Ginther, J. Appl. Phys. 47 (1976) 960.

[27] M.K. Smit, G.A. Acket and C.J. van der Laan, Thin Solid Films 138, (1986) 171.

[28] G.N. van den Hoven, E. Snoeks, A. Polman, J.W.M. van Uffelen, Y.S. Oei and M.K. Smit, Appl, Phys. Lett. 62 (1993) 3065.

[29] G.N. van den Hoven, E. Snoeks, A. Polman, J.W.M. van Uffelen and M.K. Smit, submitted to J. Appl. Phys.

[30] E. Snoeks, G.N. van den Hoven, A. Polman, B. Hendriksen, M.B.J. Diemeer and F. Priolo, J. Opt. Soc. Am. B 12 (1995), in press.

[31] G.N. van den Hoven, E. Radius, E. Snoeks and A. Polman, to be published.